

Long term sustainability of a high energy, low diversity crustal biome

Li-Hung Lin^{1,2*}, Pei-Ling Wang³, Douglas Rumble⁴, Johanna Lippmann-Pipke⁵, Erik Boice⁶, Lisa M. Pratt⁶, Barbara Sherwood Lollar⁷, Eoin L. Brodie⁸, Terry C. Hazen⁸, Gary L. Andersen⁸, Todd Z. DeSantis⁸, Duane P. Moser⁹, Dave Kershaw¹⁰, and T. C. Onstott¹

¹Department of Geosciences, Princeton University, Princeton, NJ, USA.

²Department of Geosciences, National Taiwan University, Taipei, Taiwan

³Institute of Oceanography, National Taiwan University, Taipei, Taiwan

⁴Geophysical Laboratory, Carnegie Institution of Washington, Washington, DC, USA

⁵GeoForschungsZentrum Potsdam, Telegrafenberg, Potsdam, Germany

⁶Department of Geological Sciences, Indiana University, Bloomington, IN, USA

⁷Department of Geology, University of Toronto, Toronto, ON, Canada

⁸Ecology Department, Lawrence Berkeley National Laboratory, Berkeley, CA, USA. (Work partially supported by DOE-LBNL Contract No. DE-AC02-05CH11231.)

⁹ Division of Earth and Ecosystems Sciences (DEES), Desert Research Institute, Las Vegas, NV, USA

¹⁰Mponeng Mine, Anglo Gold, Johannesburg, South Africa

*To whom correspondence should be addressed. E-mail: lhlin@ntu.edu.tw

One sentence summary: Nearly 3 km deep in the Earth's crust, a simple bacterial community has survived for millions of years on geological sources of hydrogen and sulfate

Abstract

Geochemical, microbiological and molecular analyses of alkaline, saline groundwater at 2.8 km depth in Archaean metabasalt revealed a microbial biome dominated by a single phylotype affiliated with thermophilic sulfate reducers belonging to *Firmicutes*. These sulfate reducers were sustained by geologically-produced sulfate and hydrogen at concentrations sufficient to maintain activities for millions of years with no apparent reliance upon photosynthetically-derived substrates.

Most subsurface microbial ecosystems examined to date (including subseafloor sediments, deep sea hydrothermal vents, terrestrial sedimentary aquifers and petroleum reservoirs), ultimately depend on sunlight. These studies have been mostly confined to less than 1 km depth and are either supported by photosynthetically-produced electron donors and acceptors transported by groundwater or seawater with ages much less than a million years, or in constant contact with oxygenated seawater migrating through the underlying fractured basaltic aquifer (1-4). Although two occurrences of autotrophic microbial communities have been reported to exist in <300 m deep volcanic aquifers flushed with fresh, meteoric water (5, 6), their long term sustainability on H₂ and isolation from photosynthetically-produced substrates have not been demonstrated. While the existence of subsurface microorganisms at depths greater than 1 km in pristine environments is well established (7), much still remains unknown regarding the abundance, diversity and sustainability of these microbial communities over geological time scales.

To determine the long-term sustainability of a deep terrestrial environment we examined the microbial diversity and metabolic activity of a 3-4 km-deep fracture in 2.7 Ga Ventersdorp Supergroup metabasalt for which fracture water ages of tens of millions of years (8), abundant abiogenic hydrocarbons (9), and radiolytically-produced H₂ (10) have been reported. To characterize the indigenous microbial composition and its principal respiratory pathway, we analyzed 16S rRNA genes, aqueous and gas geochemistry, and stable and noble gas isotopic signatures of moderately saline groundwater emanating from a fracture zone at 2.825 kilometers below land surface (kmbls) in the Mponeng Au mine, South Africa. This high-pressure, water-bearing fracture was intersected during exploratory drilling ahead of a tunnel advancing into an unmined zone ~100 m above the

Ventersdorp Contact Reef (VCR) ore zone. The fracture water was initially sampled as soon as it was safe to do so (4 days after the fracture intersection), and 3 subsequent samples were obtained over a 54-day interval (Table 1) to monitor drilling contamination and possible changes of community structure and geochemistry as the fracture was dewatered and prior to sealing by the mine's cementation team.

Fracture water samples yielded a uniform community structure dominated by a single phylotype (MP104-0916-b1) that comprised >88% of the clones in 16S rDNA libraries, but did not appear in the water used for mining (Fig. 1a). This phylotype was related (96% similarity) to an uncultured clone recovered from thermal fluids of oceanic crust (11) or *Desulfotomaculum kuznetsovii* (91% similarity) (12), a sulfate reducer growing at moderately thermophilic conditions. Of the other minor bacterial and archaeal phylotypes associated with the fracture water, MP104-1109-a19 resembled (98% similarity) environmental clones (SAGMEG-2 group) obtained from fracture water in an adjacent mine (13) (Fig. 1b). Other phylotypes were closely related (98 - 99% similarity) to environmental clones recovered from surface environments (such as soils and sludge) or to various mesophiles distributed within *Proteobacteria*, *Firmicutes*, and *Methanobacteria* (Fig. 1). These minor phylotypes did not resemble those from the mining water (supporting online material; SOM).

High-density 16S rDNA microarray analysis was also used as a more sensitive approach to assess microbial diversity. Array hybridization results supported the finding that microbial diversity was much less (Table S2) and the *Firmicutes* were of greater relative abundance (Table S3) in the fracture water than the mining water. Some overlap

between the sequences found in the fracture water and those of the mining water is expected because mining water is a mixture of recycled fracture water and surface water.

The geochemistry of the fracture water was characterized to identify its origin and to assess the principal metabolic pathways (Tables 1, S1 and S4). Over the observation period, the temperature decreased from $>60^{\circ}\text{C}$ to 52°C ; while the pH was constant and the redox potential (Eh) increased from -330 to -263 mV. The Cl^- , Br^- and SO_4^{2-} concentrations increased significantly, whereas other anion concentrations fluctuated or decreased slightly. Reduced gases (H_2 and CH_4) were abundant (> 1 mM) and their concentrations increased as water flow rates declined and gas flow rates remained constant. Formate and acetate ranged from 7 to 9 μM and 22 to 36 μM , respectively. The $\delta^2\text{H}$ and $\delta^{13}\text{C}$ of the abundant, dissolved C_{1-4} hydrocarbons indicated an abiogenic origin based on their similarity to abiogenic hydrocarbon gases identified at other Precambrian Shield sites (9). The $\delta^2\text{H}$ and $\delta^{18}\text{O}$ values of the fracture water, -29.1‰ and -6.9‰ VSMOW (Vienna Standard Mean Ocean Water), respectively, plotted slightly above the global and local meteoric line (14). The $\delta^2\text{H}\text{-H}_2$ ranged between -680 and -690‰ VSMOW, which when compared with the $\delta^2\text{H}\text{-H}_2\text{O}$ yielded isotopic equilibrium temperatures of 62°C for the first sample declining to 49°C for the last sample. Based upon the thermal conductivity model (15) and the heat flow data (16), the initial temperature equates to that at 4.2 kmbls and the final temperature to that at 2.9 kmbls.

Noble gas analyses yielded elevated radiogenic and fissionogenic concentrations of ^4He , ^{40}Ar , ^{134}Xe and ^{136}Xe (Table S1) but exhibited no systematic trend during the observation period. The bulk model age of the fracture water ranged from (15.8 ± 7.9) Ma to (25.0 ± 3.8) Ma (Table 1). This model age represents either the true subsurface residence

time or the mixing between an ancient (0.8 to 2.5 Ga), saline, H₂, C₁₋₄ and sulfate-rich, hydrothermal fluid with a ~3 to 4 Ma old, moderately saline, H₂, C₁₋₄ and sulfate-poor, paleometeoric water (SOM).

The exceptional dominance of the *Firmicutes* clones, distinct $\delta^2\text{H}$ and $\delta^{18}\text{O}$ values of the fracture water from those of the mining water (17), and the increasing H₂, CH₄, He, Cl⁻, Br⁻ and SO₄²⁻ concentrations during the observation period suggests that the fracture environment favors their survival and that mining operations had minimal impact on this environment during depressurization and dewatering. *Desulfotomaculum*-related environmental clones and isolates have been detected from other subsurface environments, including an oil reservoir (18), deep sedimentary strata (19, 20), an ore deposit (21), and saline water emanating from a 3.2-kmbls borehole located 13 km east of this borehole (22). The evident success of these microorganisms may not be surprising since their ability to form endospores would facilitate their survival during periods of low water activity, nutrient deprivation, and sub-optimal temperature (23). Whether the less abundant members of the clone libraries represent indigenous microorganisms that are capable of acquiring energy through metabolisms distinct from those strains they most resemble phylogenetically, or alternatively represent moribund relics of shallower, less saline paleometeoric water that has mixed with this fracture water is not known.

Sulfur isotopic analyses yielded $\delta^{34}\text{S}$ values of HS⁻ ranging from 11‰ to 13‰ Vienna Canon Diablo Meteorite (VCDT), and those of SO₄²⁻ from 19‰ to 26‰ VCDT (Table S4). The depleted $\delta^{34}\text{S}$ value of HS⁻ relative to that of SO₄²⁻ (-7.7‰ for sample #4 and -12.4‰ for sample #7) is consistent with microbial sulfate reduction. The fact that SO₄²⁻ concentrations in the fracture water were higher than that of the overlying dolomitic

aquifer (13), and that SO_4^{2-} has been reported in analyses of fluid inclusions from hydrothermal quartz in the VCR (24) and the reservoir mixing-fractionation model (SOM) all suggest that SO_4^{2-} originated from the ancient hydrothermal fluid, not the paleometeoric end member. The $\delta^{34}\text{S}$ values of fracture pyrite (0‰ to 2‰ VCDT) were less than that of the coexisting barite (10.1‰ VCDT) (Table S4) and were consistent with those of hydrothermal 2.0 Ga pyrite from the VCR in the same mine (25). The $\Delta^{33}\text{S}$ values for all samples clustered around 0‰ (Table S4). To reproduce the $\Delta^{33}\text{S}$ of total dissolved S species (-0.022‰) for sample #7, a mixing of sulfate derived from pyrite oxidation and barite dissolution with a Rayleigh isotopic fractionation by microbial sulfate reduction was required (SOM). Such a mixture comprised of 30% SO_4^{2-} derived from oxidation of pyrite by radiolytically-produced oxidants (10) and 70% SO_4^{2-} from the dissolution of barite and produced an initial $\delta^{34}\text{S}$ value of 8.13‰ VCDT and a $\Delta^{33}\text{S}$ value of -0.0087‰ (SOM). The isotopic evolution from initial 8.13‰ VCDT to the present observation (18.63‰ VCDT for total dissolved S species) requires a Rayleigh fractionation process where 70% of the initial SO_4^{2-} was removed as microbially-precipitated pyrite (SOM). By this model the total HS^- formed by microbial sulfate reduction would be 4.35 mM ($1.52 \text{ mM} \times 70\% / 30\% + 0.80 \text{ mM HS}^-$; SOM).

The Gibbs free energy for microbial redox reactions was calculated to provide additional constraints on the dominant respiratory pathway occurring in this fracture water. Sulfate reduction dominated the free energy yields for a wide range of electron donor and acceptor combinations (Table 2). The free energy yields for these reactions were much greater than the minimum requirement for synthesis of 1/3 ATP molecule by pumping one proton across the membrane ($\sim 20 \text{ kJ}$) (26). Among electron donors available for sulfate

reduction and methanogenesis, H₂ yielded more free energy than acetate and formate, and H₂-utilizing sulfate reduction yielded the highest free energy and energy flux (Table 2), suggesting that CO₂-utilizing methanogens and acetogens cannot sustain as high a population density as sulfate reducers and therefore would be minor constituents of the community, as is observed in the clone libraries. The prominence of the free energy flux for H₂-utilizing sulfate reduction over other metabolic reactions is consistent with the depletion of δ³⁴S values of HS⁻ relative to SO₄²⁻ (27) and the physiological characteristics inferred from the dominant phylotype.

The in situ rate of microbial sulfate reduction was estimated to range from 0.22 to 1.45 nM yr⁻¹, or from 5.5×10⁻¹⁸ to 3.6×10⁻¹⁷ moles cell⁻¹ yr⁻¹ (assuming all observed cells, 4×10⁷ cells L⁻¹, actively reduce SO₄²⁻) based upon the potential microbially-produced sulfide (4.35 mM; SOM) and fracture water residence time of ~3 or ~20 Ma inferred from noble gas analysis. Such a rate is comparable to rates reported in subseafloor sediments (28) and to the estimated rate of radiolytic H₂ generation (10), but far less (4 to 5 orders of magnitude) than the maintenance energy demand of mesophilic sulfate reducers as determined in laboratory experiments (29) (SOM). The estimated in situ sulfate reduction rate when combined with the experimental maintenance energy demand (48 moles (g dry wt. cell)⁻¹ yr⁻¹) (29) and assuming a 20 femtograms cell⁻¹ would only support 200 to 1600 cells L⁻¹, which is far below the observed ~4×10⁷ cells L⁻¹. If cells were constantly growing and dying, then the experimental sulfate reducer yield of 12.2 g dry wt. mole⁻¹ (29) when combined with the in situ sulfate reduction rate would correspond to cell turnover times of 45-300 years. The isotopic estimate of the long-term in situ microbial activity, however, is 10⁹-10¹⁰ less than the maximum substrate consumption rate (Table 2), which

would seem to indicate that as yet unidentified factors play a role in restraining the microbial respiration.

The hot, reducing, gaseous water emanating from a fracture at 2.8 to 4.2 kmbls harbored a microbial community dominated by a single *Firmicutes* phylotype. The *Firmicutes* probably penetrated the Mponeng fracture zone at current depths during infiltration of paleometeoric water between 3 and 25 Ma and since then have relied upon non-photosynthetically-derived H₂ and SO₄²⁻ converted from Archaean/Proterozoic pyrite/barite. Nutrient concentrations have remained much higher than observed in shallower crustal environments, suggesting that the deep crustal biosphere may be energy rich, is not approaching entropic death and is capable of sustaining microbial communities indefinitely by geological processes.

References and notes

1. K. O. Stetter *et al.*, *Nature* **365**, 743 (1993).
2. D. M. Karl, in *The Microbiology of Deep-Sea Hydrothermal Vents* D. M. Karl, Ed. (CRC Lewis Publishers, Boca Raton, FL, 1995) pp. 35-124.
3. E. M. Murphy *et al.*, *Water Res. Res.* **28**, 723 (1992).
4. S. D'Hondt *et al.*, *Science* **306**, 2216 (2004).
5. F. H. Chapelle *et al.*, *Nature* **415**, 312 (2002).
6. T. O. Stevens, J. P. McKinley, *Science* **270**, 450 (1995).
7. T. C. Onstott *et al.*, in *Enigmatic microorganisms and life in extreme environments* J. Seckbach, Ed. (Kluwer Academic Publishers, Netherlands, 1999) pp. 489-500.
8. J. Lippmann *et al.*, *Geochim. Cosmochim. Acta* **67**, 4597 (2003).
9. B. Sherwood Lollar *et al.*, *Chem. Geol.* **226**, 328 (2006).
10. L. H. Lin *et al.*, *Geochem. Geophys. Geosyst.* **6**, Q07003 doi:10.1029/2004GC000907 (2005).
11. J. P. Cowen *et al.*, *Science* **299**, 120 (2003).
12. T. N. Nazina, A. E. Ivanova, L. P. Kanchaveli, E. P. Rozanova, *Mikrobiologiya* **57**, 823 (1988).
13. K. Takai, D. P. Moser, M. DeFlaun, T. C. Onstott, J. K. Fredrickson, *Appl. Environ. Microbiol.* **67**, 5750 (2001).
14. H. Craig, *Science* **133**, 1702 (1961).
15. G. Omar, T. C. Onstott, J. Hoek, *Geofluids* **3**, 69 (2003).

16. M. Q. W. Jones, *J. Geophys. Res.* **93**, 3243 (1988).
17. G. R. Drennan, M. C. Boiron, M. Cthelineau, L. J. Robb, *Mineral. Petrol.* **66**, 83 (1999).
18. C. Tardy-Jacquenod, M. Magot, B. K. Patel, R. Matheron, P. Caumette, *Int. J. Syst. Bacteriol.* **48**, 333 (1998).
19. H. Saas, H. Cypionka, *Syst. Appl. Microbiol.* **27**, 541 (2004).
20. Y. Liu *et al.*, *Int. J. Syst. Bacteriol.* **47**, 615 (1997).
21. T. Nakagawa *et al.*, *FEMS Microbiol. Ecol.* **41**, 199 (2002).
22. D. P. Moser *et al.*, *Gemicrobiol. J.* **20**, 517 (2003).
23. L. L. Campbell, R. Singleton, in *Bergey's Manual of Systematic Bacteriology* P. H. A. Sneath, N. S. Mair, M. E. Sharpe, J. G. Holt, Eds. (Williams & Wilkins, Baltimore, 1986), vol. 2, pp. 1200-202.
24. H. E. Frimmel, D. K. Hallbauer, V. H. Gartz, *Mineral. Petrol.* **66**, 55 (1999).
25. B. Zhao, C. Harris, L. J. Jordaan, L. J. Robb, *Geoscience Africa 2004* **2**, 732 (2004).
26. B. Schink, *Microbiol. Mol. Biol. Rev.* **61**, 262 (1997).
27. A. L. W. Kemp, H. G. Thode, *Geochim. Cosmochim. Acta* **32**, 71 (1968).
28. R. J. Parkes *et al.*, *Nature* **436**, 390 (2005).
29. W. Badziong, R. K. Thauer, *Arch. Microbiol.* **117**, 209 (1978).
30. This work was supported by NSF and NASA LExEn to T.C.O., NSC to L.-H.L. and P.-L.W., JPL, NASA Cosmochemistry NAG5 and NSF EAR to D.R., DFG to J.L.-P., NASA NAI (IPTAI) to L.P., NSERC and Killam Fellowship funds to B.S.L., and DOE GTL to T.C.H. We thank the team members of the Witwatersrand Microbiology Project and geologists of the Mponeng mine for their assistance of field sampling and coordination of logistic supply. We also acknowledge G. Southam, G. Wagner, B. Tipple, T. Gihring, E. Van Heerden and D. Litthauer (Univ. of Free State) for providing laboratory space and assisting with sample collection, and R. Wilson (SRK-Turgis Tech.) for setup of the field laboratory and logistical assistance. Genbank accession numbers for sequences are from DQ088779 to DQ088817.

Table 1. Geochemical and microbiological characteristics of fracture water and mining water.

| Sample No. (number of days since intersection) | 1 (4) | 2 (7) | 3 (15) | 4 (58) | 5 |
|--|-------------------------|-----------------------|-----------------------|-------------------------|--------------------------|
| Sample name | MP104E65X C-091602 | MP104E65X C-091902 | MP104E65X C-092702 | MP104E65X C-110902 | MP104E65XC- SW-091602 |
| Origin | Fracture water | Fracture water | Fracture water | Fracture water | Mining water |
| Water and gas flow rates (L min ⁻¹) (borehole volumes) | 40/2.4 (45) | 10.9/0.8 (55) | 8.2/1.2 (64) | 2.3/1.7 (96) | NA |
| pH | 9.3 | 9.3 | 9.3 | 9.2 | NA |
| Eh (mV) | -330 | -350 | -340 | -263 | NA |
| Temperature (°C) | >60 | 52 | 52 | 52 | 20 |
| Formate (μM) | 7.6 | NA | 7.1 | 8.9 | 1.4 |
| Acetate (μM) | 24.6 | NA | 22.5 | 35.7 | 5.9 |
| Cl ⁻ (mM) ¹ | 54.1 | NA | 71.9 | 84.9 | 0.42 |
| Br ⁻ (μM) | 125 | NA | 177 | 218 | 3.8 |
| SO ₄ ²⁻ (μM) | 529 | NA | 900 | 1860 | 171 |
| HS ⁻ (μM) ² | NA | 1390 | NA | 1060 | NA |
| H ₂ (μM) ² | 1940 | 2600 | 2090 | 3715 | NA |
| CH ₄ (μM) ² | 8580 | 11800 | 9320 | 16600 | NA |
| O ₂ (μM) ³ | 6 | <d.l. ³ | <d.l. | <d.l. | 285 |
| δ ² H-H ₂ (‰VSMOW) | -684 | -684 | -688 | -695 | NA |
| δ ¹³ C-CH ₄ (‰PDB) | -31.6 | -31.7 | -32.8 | -33.2 | NA |
| δ ² H-CH ₄ (‰VSMOW) | -364 | -367 | -366 | -390 | NA |
| ⁴ He model age (Ma) | 20.9±10.5 | 20.4±10.2 | 15.8±7.9 | NA | NA |
| ⁴⁰ Ar model age (Ma) | 16.3±8.2 | 21.3±10.6 | 16.9±8.4 | NA | NA |
| ¹³⁴ Xe model age (Ma) | 18.7±7.0 | 19.4±3.8 | 21.0±6.0 | NA | NA |
| ¹³⁶ Xe model age (Ma) | 21.6±6.0 | 25.0±3.8 | 23.8±4.6 | NA | NA |
| Bacterial DNA (pg ml ⁻¹) | 15±8 | 16±8 | 30±15 | 30±15 | 3±1.5×10 ⁵ |
| Archaeal DNA (pg ml ⁻¹) | ~5E-4 | <d.l. | ~5E-4 | ~5E-4 | 206±100 |
| Cell density (cells ml ⁻¹) | 5.1±0.5×10 ⁴ | NA | NA | 3.3±0.3×10 ⁴ | NA |

¹The concentrations derived from charged balance were 10.2 mM for sample #1, 27.6 mM for sample #3 and 50.6 mM for sample #4, respectively.

²The concentrations of dissolved gases were reported as concentrations corrected for diffusive loss (8). Diffusive correction was not applied to sample #4 due to the lack of noble gas analysis.

³The positive O₂ content for sample #1 may be derived from incomplete isolation of fracture water from the mining environment caused by the extremely high water pressure and flow rate.

⁴Carbon isotopic value was referenced to Pee Dee Belemnite (PDB).

⁵The uncertainties for aqueous and gas chemistry are ±10% and ±20%, respectively. The uncertainties for isotopic measurements are ±0.5‰ for δ¹³C-hydrocarbon and ±5‰ for δ²H-hydrocarbon and δ²H-H₂, respectively.

⁶NA: not available; <d.l.: below detection limit, which is 1 μM for O₂ and 0.5 fg ml⁻¹ for archaeal DNA.

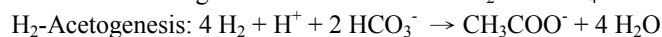
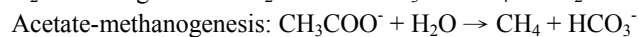
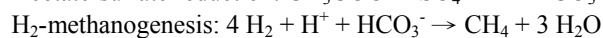
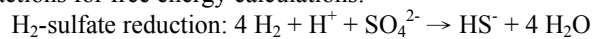
Table 2. Gibbs free energy, substrate consumption rate¹ and steady state free energy flux¹, FEF, for various microbial redox reactions.

| Sample No. | 1 | | | 3 | | | 4 | | |
|--------------------------------------|--|--|--|--|--|--|--|--|--|
| | ΔG kJ mole ⁻¹ | Substrate rate $\mu\text{M yr}^{-1}$ | Energy flux kJ cell ⁻¹ sec ⁻¹ | ΔG kJ mole ⁻¹ | Substrate rate $\mu\text{M yr}^{-1}$ | Energy flux kJ cell ⁻¹ sec ⁻¹ | ΔG kJ mole ⁻¹ | Substrate rate $\mu\text{M yr}^{-1}$ | Energy flux kJ cell ⁻¹ sec ⁻¹ |
| H ₂ -sulfate reduction | -148 | 5.9E+06 | -9.2E-13 | -155 | 8.6E+06 | -1.4E-12 | -146 | 1.8E+07 | -2.7E-12 |
| Acetate-sulfate reduction | -86 | 1.9E+05 | -1.7E-14 | -94 | 1.5E+05 | -1.5E-14 | -82 | 2.4E+05 | -2.1E-14 |
| H ₂ - methanogenesis | -94 | 2.1E+05 | -2.1E-14 | -95 | 2.9E+04 | -2.9E-15 | -93 | 3.8E+05 | -3.7E-14 |
| Acetate- methanogenesis | -33 | 1.9E+05 | -6.6E-15 | -34 | 1.5E+05 | -5.5E-15 | -28 | 2.4E+05 | -7.1E-15 |
| Formate- methanogenesis | -74 | 1.8E+04 | -1.4E-15 | -86 | 1.5E+04 | -1.3E-15 | -42 | 1.8E+03 | -8.1E-17 |
| H ₂ -Acetogenesis | -62 | 1.4E+05 | -9.3E-15 | -61 | 2.0E+04 | -1.2E-15 | -64 | 2.5E+05 | -1.7E-14 |

¹The calculation for maximum substrate consumption rate and steady state free energy flux is shown in SOM.

²The HS⁻ concentration used in the calculation for sulfate reduction for samples #1 and #3 were assumed to be 1.3 mM. The free energy for sulfate reduction only varied less than 5% when HS⁻ concentration was changed between 1.1 to 1.5 mM.

³The reactions for free energy calculations:



⁴The uncertainties are $\pm 10\%$.

Figure legends

Figure 1. Phylogenetic trees for bacteria (a) and archaea (b) based on 16S rDNA sequences recovered from fracture and mining water in the Mponeng Au mine, South Africa. The fraction number in the parenthesis represents the number of clones for each phylotype versus the total number of clones analyzed in each sample. The bar is equivalent to the sequence variation of 10%.